

# Consistent LDA'+DMFT approach to electronic structure of transition metal oxides: charge transfer insulators and correlated metals.

<sup>1</sup>I.A. Nekrasov, <sup>1</sup>N.S. Pavlov, <sup>1,2</sup>M.V. Sadovskii

<sup>1</sup>*Institute for Electrophysics, Russian Academy of Sciences, Ural Branch, Amundsen str. 106, Ekaterinburg, 620016, Russia*

<sup>2</sup>*Institute for Metal Physics, Russian Academy of Sciences, Ural Branch, S. Kovalevskaya str. 18, Ekaterinburg, 620990, Russia*

We discuss the recently proposed LDA'+DMFT approach providing consistent parameter free treatment of the so called double counting problem arising within the LDA+DMFT hybrid computational method for realistic strongly correlated materials. In this approach the local exchange-correlation portion of electron-electron interaction is excluded from self consistent LDA calculations for strongly correlated electronic shells, e.g.  $d$ -states of transition metal compounds. Then the corresponding double counting term in LDA'+DMFT Hamiltonian is consistently set in the local Hartree (fully localized limit - FLL) form of the Hubbard model interaction term. We present the results of extensive LDA'+DMFT calculations of densities of states, spectral densities and optical conductivity for most typical representatives of two wide classes of strongly correlated systems in paramagnetic phase: charge transfer insulators (MnO, CoO and NiO) and strongly correlated metals (SrVO<sub>3</sub> and Sr<sub>2</sub>RuO<sub>4</sub>). It is shown that for NiO and CoO systems LDA'+DMFT qualitatively improves the conventional LDA+DMFT results with FLL type of double counting, where CoO and NiO were obtained to be metals. We also include in our calculations transition metal  $4s$ -states located near the Fermi level missed in previous LDA+DMFT studies of these monooxides. General agreement with optical and X-ray experiments is obtained. For strongly correlated metals LDA'+DMFT results agree well with earlier LDA+DMFT calculations and existing experiments. However, in general LDA'+DMFT results give better quantitative agreement with experimental data for band gap sizes and oxygen states positions, as compared to the conventional LDA+DMFT.

PACS numbers: 71.20.-b, 71.27.+a, 71.28.+d, 74.25.Jb

## I. INTRODUCTION

During last decade the LDA+DMFT method (local density approximation + dynamical mean-field theory) became probably the most powerful tool to calculate electronic structure of real strongly correlated materials [1–6]. Typically this approach consists of two computation steps. First, LDA calculations are exploited to obtain the non-interacting Hamiltonian  $\hat{H}^{\text{LDA}}$  which describes, rather accurately, the kinetic energy (and to some extent takes into account electronic interactions). At the second step the local Coulomb (Hubbard) interaction  $\hat{H}^{\text{Hub}}$  is introduced into the lattice problem defined by  $\hat{H}^{\text{LDA}}$  for those electronic shells which are supposed to be strongly correlated. Thus obtained generalized Hubbard model is solved numerically using DMFT. Some attempts to organize a feedback from DMFT step back to LDA calculations to achieve fully self-consistent LDA+DMFT are also known and may be important for some physical problems [7].

The double counting problem arises in the standard LDA+DMFT, because some portion of local electron-electron interaction for correlated shells is actually accounted for within  $\hat{H}^{\text{LDA}}$ . To avoid this double counting it is necessary to subtract a certain correction term  $\hat{H}^{\text{DC}}$  from  $\hat{H}^{\text{LDA}}$ . Then the formal LDA+DMFT Hamiltonian is written as:

$$\hat{H} = \hat{H}^{\text{LDA}} + \hat{H}^{\text{Hub}} - \hat{H}^{\text{DC}}. \quad (1)$$

In orbital space  $\hat{H}^{\text{DC}}$  is the diagonal matrix with non zero and equal matrix elements  $E_{dc}$  for these atomic shells assumed to be strongly (e.g.  $d$  or  $f$  shells or their subshells). This becomes more transparent if we consider the corresponding Green's function for the Hubbard model:

$$\hat{G}_{ij}(\mathbf{k}E) = [(E - \mu)\hat{I} - H_{ij}^{\text{LDA}}(\mathbf{k}) - (\Sigma(\mathbf{k}E) - E_{dc})\delta_{id}\delta_{jd}]^{-1}, \quad (2)$$

where  $\hat{I}$  is the unity matrix in the orbital space,  $\mu$  is the chemical potential and  $\Sigma(\mathbf{k}E)$  is the self-energy corresponding to local Coulomb (Hubbard) interaction, [...] <sup>-1</sup> denotes matrix inversion, while index  $d$  denotes correlated states for which Coulomb (Hubbard) interaction is taken into account.

From Eq. (2) one can see that in case of  $\hat{H}^{\text{LDA}}$  containing only the contribution of interacting  $d$ -orbitals,  $E_{dc}$  reduces to trivial renormalization of the chemical potential  $\mu$ . Then, strictly speaking, there is no double counting problem at all. Because of this many of early works (listed e.g. in reviews [2,4–6], except probably the first paper on LDA+DMFT [1] and few others) just dropped the double counting correction term. Only after the LDA+DMFT community started the active studies of multiband  $\hat{H}^{\text{LDA}}$  Hamiltonians with both correlated and non correlated states included, the problem of correct implementation of  $\hat{H}^{\text{DC}}$  became important. Now there are dozens of works devoted to multiband LDA+DMFT studies. Important classes of materials investigated can be listed as:

1. Transition metal oxides (LaTiO<sub>3</sub>, (Sr,Ca)VO<sub>3</sub>, V<sub>2</sub>O<sub>3</sub>, VO<sub>2</sub>, CrO<sub>2</sub>, LaMnO<sub>3</sub>, NiO, MnO, CoO, FeO, LaCoO<sub>3</sub>, TiOCl, Tl<sub>2</sub>Mn<sub>2</sub>O<sub>7</sub>, LaNiO<sub>3</sub>, (Ca,Sr)<sub>2</sub>RuO<sub>4</sub>, Na<sub>0.3</sub>CoO<sub>2</sub>);
2. Elemental transition metals and non-oxide transition metal compounds (Cr, Mn, Fe, Ni, Co, multilayers (CrAs)/(GaAs), NiMnSb, Co<sub>2</sub>MnSi, CrAs, VAs, ErAs, Ni(S,Se)<sub>2</sub>, KCuF<sub>3</sub>);
3. Elemental *f*-electron materials and their compounds (Ce, Pu, Am, Ce<sub>2</sub>O<sub>3</sub>, Pu<sub>2</sub>O<sub>3</sub>, USe, UTe, PuSe, PuTe, PuCoGa<sub>5</sub>, URu<sub>2</sub>Si<sub>2</sub>, CeIrIn<sub>5</sub>, CeCoIn<sub>5</sub>, CeRhIn<sub>5</sub>);
4. Nano materials (Ni-Cu nano contacts and nano electrodes);
5. High temperature copper superconductors ((Sr,La)<sub>2</sub>CuO<sub>4</sub>, (Pr,Ce)<sub>2</sub>CuO<sub>4</sub>, Bi<sub>2</sub>Ca<sub>2</sub>SrCuO<sub>8</sub> etc.);
6. Superconducting iron pnictides (LaFeAsO, Ce-FeAsP, LiFeAs, BaFe<sub>2</sub>As<sub>2</sub>, etc.).

These systems show a large variety of physical effects. Among them there are strongly correlated metals, Mott and charge transfer insulators, ferromagnets and antiferromagnets, superconductors, etc. However, up to now there is no universal and unambiguous expression for  $\hat{H}^{DC}$ , and different formulations are used for different classes of materials.

In this paper we present the results of extensive application of our recently proposed LDA'+DMFT [12] approach to charge transfer insulators MnO, CoO and NiO and strongly correlated metals SrVO<sub>3</sub> and Sr<sub>2</sub>RuO<sub>4</sub>, confronted to conventional LDA+DMFT results and some experiments. The manuscript has following structure. In Sec. II we present an overview of different definitions of the  $\hat{H}^{DC}$ . The novel consistent LDA'+DMFT method is described in Sec. III. LDA and LDA' band structures, total and partial densities of states, spectral density maps and optical conductivity LDA'+DMFT results for prototype charge transfer insulators MnO, NiO and CoO are presented in Sec. IV and compared with the results of conventional LDA+DMFT. These results are further compared with experimental data on X-ray spectroscopy and optical conductivity. In Sec. V we discuss LDA and LDA' band structures for correlated metallic systems prototypes SrVO<sub>3</sub> and Sr<sub>2</sub>RuO<sub>4</sub> are presented. Then LDA+DMFT and LDA'+DMFT results are compared with each other and with experimental photoemission and absorption spectra. Finally we end up with the Conclusion (Sec. VI).

## II. REVIEW OF DIFFERENT FORMULATIONS FOR $\hat{H}^{DC}$

To derive an expression for  $\hat{H}^{DC}$  let us examine  $\hat{H}^{LDA}$  and  $\hat{H}^{Hub}$  terms Eq. (1). LDA part of the Hamiltonian

(1) is given by:

$$\hat{H}_{LDA} = -\frac{\hbar^2}{2m_e}\Delta + V_{ion}(\mathbf{r}) + \int d^3r' \rho(\mathbf{r}')V_{ee}(\mathbf{r}-\mathbf{r}') + \frac{\delta E_{xc}^{LDA}(\rho)}{\delta\rho(\mathbf{r})}, \quad (3)$$

where  $\Delta$  is the Laplace operator,  $m_e$  the electron mass,  $e$  the electron charge, and

$$V_{ion}(\mathbf{r}) = -e^2 \sum_i \frac{Z_i}{|\mathbf{r}-\mathbf{R}_i|}, \quad V_{ee}(\mathbf{r}-\mathbf{r}') = \frac{e^2}{2} \sum_{\mathbf{r} \neq \mathbf{r}'} \frac{1}{|\mathbf{r}-\mathbf{r}'|} \quad (4)$$

denote the one-particle potential due to all ions  $i$  with charges  $eZ_i$  at given positions  $\mathbf{R}_i$ , and the electron-electron interaction, respectively.

The  $E_{xc}^{LDA}(\rho(\mathbf{r}))$  in (3) is some function of local charge density, which approximates the true exchange correlation functional  $E_{xc}[\rho]$  of density functional theory within local density approximation [8]. The explicit expression for  $E_{xc}^{LDA}(\rho(\mathbf{r}))$  is usually derived from perturbation theory [9] or numerical simulations [10] of the ‘‘jellium’’ model with  $V_{ion}(\mathbf{r}) = \text{const}$ . To obtain the value of local charge density one should choose some basis set of one-particle wave functions  $\varphi_i$  (e.g. to do practical calculations and explicitly express matrix elements of the Hamiltonian (3)), so that  $\rho(\mathbf{r})$  is written as:

$$\rho(\mathbf{r}) = \sum_{i=1}^N |\varphi_i(\mathbf{r})|^2. \quad (5)$$

Hubbard-like (local) interaction term including direct Coulomb interaction and exchange Coulomb interaction contributions in the density-density form is written as:

$$\hat{H}^{Hub} = U \sum_m \sum_i \hat{n}_{im\uparrow} \hat{n}_{im\downarrow} + \sum_i \sum_{m \neq m'} \sum_{\sigma\sigma'} (U' - \delta_{\sigma\sigma'} J) \hat{n}_{im\sigma} \hat{n}_{im'\sigma'}. \quad (6)$$

Here, the index  $i$  enumerates lattice sites,  $m$  denotes orbitals, and  $\sigma$  the spin. The  $U$  represents local intra-orbital Coulomb repulsion and  $J$  -  $z$ -component of Hund's rule coupling between the strongly correlated electrons (e.g.  $d$ -states, enumerated by  $i = i_d$  and  $l = l_d$ ). Rotational invariance then fixes the local inter-orbital Coulomb repulsion  $U' = U - 2J^{11}$ . The values of  $U$  and  $J$  are obtained usually from constrained LDA procedure [15]. One can get numerically exact solution of the Hubbard Hamiltonian (simplified kinetic term plus  $\hat{H}^{Hub}$  term) within DMFT approximation.

Hamiltonian  $\hat{H}_{LDA}$  contains local electron-electron correlations through the exchange correlation energy (taken in the form valid for uniform electronic gas) and density-density contribution of the Hartree term. In its turn, DMFT provides the numerical solution of the Hubbard

model (exact in infinite dimensions). Thus it is clear that before plugging  $\hat{H}_{\text{LDA}}$  into DMFT lattice problem (2), one must subtract certain double counting correction term  $\hat{H}^{DC}$  from  $\hat{H}_{\text{LDA}}$ . The double counting *problem* arises because there is no explicit microscopic or diagrammatic relation between the model (Hubbard like) Hamiltonian approach and LDA. There is apparently no possibility to give a rigorous expression for  $\hat{H}^{DC}$  in terms of  $U$ ,  $J$  and  $\rho$ . Thus, several *ad hoc* expressions for  $\hat{H}^{DC}$  and approaches to treat the double counting problem exist in the current literature. Below we briefly discuss some of these derivations.

Perhaps for the first time problem of double counting appeared within an attempt to merge LDA and the Hubbard model within the LDA+U method [13], where was initially *postulated* the so called “around mean-field” (AMF) definition of  $\hat{H}^{DC}$ . This definition comes from an assumption that LDA is a kind of “mean-field” solution of the Hubbard-like problem Eq. (6). Later on the definition of Ref. [13] was generalized for spin dependent (LSDA) case (and even more general – with matrix form of Coulomb interaction). After this spin dependent generalization corresponding AMF expression can be given as:

$$\hat{H}_{\text{AMF}}^{DC} = \frac{1}{2}U \sum_{\sigma} n_{d\sigma}(n_d - n_{\sigma}^0) - \frac{1}{2}J \sum_{\sigma} n_{d\sigma}(n_{d\sigma} - n_{\sigma}^0) \quad (7)$$

with the average occupancies  $n^0 = \frac{1}{2(2l+1)} \sum_{m,\sigma} n_{m\sigma}$ ,  $n_{\sigma}^0 = \frac{1}{(2l+1)} \sum_m n_{m\sigma}$  and total number of electrons on interacting orbitals (per spin projection)  $n_{d\sigma} = \sum_m n_{il_d m\sigma} = \sum_m \langle \hat{n}_{il_d m\sigma} \rangle$  and  $n_d = \sum_{\sigma} n_{d\sigma}$ . originally supposed to be found from LDA calculations. The drawback of AMF is the equal occupancy of all orbitals which is not correct even for weakly correlated systems because e.g. of crystal field splitting. However, a couple of the modern LDA+DMFT works reported the reasonable results with AMF-like double counting correction term. Apparently, the AMF double counting correction works rather well for moderately correlated metallic systems. Some modifications of (7) were given in Refs. [16] and applied to LDA+DMFT calculations for charge transfer insulators.

Later on the fully localized (or atomic) limit (FLL) expression for  $\hat{H}^{DC}$  was introduced in Refs. [14,17] (with first application to LDA+DMFT calculations in Ref. [1]):

$$\hat{H}_{\text{FLL}}^{DC} = \frac{1}{2}U n_d(n_d - 1) - \frac{1}{2}J \sum_{\sigma} n_{d\sigma}(n_{d\sigma} - 1). \quad (8)$$

The Eq. (8) actually represents the Hartree decoupling of the Hubbard model interaction term (6) — decoupling of the density-density term  $\hat{n}_i \hat{n}_j$  and not full four operator term  $\hat{c}_i^{\dagger} \hat{c}_j^{\dagger} \hat{c}_o \hat{c}_i$ . Thus strictly speaking in Eq. (8) there is no Fock type of contribution since Hund exchange is presented in Eq. (6) in the density-density form, although Hund coupling value  $J$  has “exchange nature”. Quite

often it is misinterpreted as due to the “true” Hartree-Fock decoupling of  $\hat{c}_i^{\dagger} \hat{c}_j^{\dagger} \hat{c}_o \hat{c}_i$  term.

The FLL expression in the context of LDA+DMFT calculations was used in the majority of modern works. It works reasonably good for both metallic and insulating strongly correlated materials. Recently some modifications of FLL were proposed in Refs. [18,19]. Typically these modifications are used to quantitative improvements of LDA+DMFT results for particular compounds. Some kind of AMF and FLL “hybrid scheme” was used in Ref. [20] for  $\alpha - \text{Fe}$ .

Alternative way to derive or guess the  $\hat{H}^{DC}$  term is to express it through the characteristics of intrinsic single DMFT impurity problem, such as impurity self-energy  $\Sigma_{mm'}^{imp}$  or impurity Green’s function  $G_{mm'}^{imp}$ . A popular way is to define double counting energy as a static part of the impurity self-energy [21]:

$$E_{dc} = \frac{1}{2} \text{Tr}_{\sigma} (\Sigma_{\sigma}^{imp}(0)). \quad (9)$$

Some of LDA+DMFT papers used this definition in calculations of metallic magnetic and non-magnetic systems. From the very beginning this type of double counting correction was also exploited within the GW+DMFT approach [22].

Hartree energy can be determined from LDA+DMFT self-energy as its real part in the high frequency limit value. In Ref. [25] it was proposed to use thus defined Hartree energy as a double counting correction, using the constraint

$$\text{ReTr}(\Sigma_{mm'}^{imp}(i\omega_N)) = 0, \quad (10)$$

where  $\omega_N$  is the highest Matsubara frequency (used in calculations). Physically similar definition of double counting term  $E_{dc} = \Sigma(\omega \rightarrow \infty)$  was successfully applied to metallic ferromagnetic  $\text{SrCoO}_3$ [23].

For metallic systems it was suggested to fix the double counting correction by equating the number of particles of non-interacting problem and impurity problem as expressed via corresponding Green’s function [24]:

$$\text{Tr} G_{mm'}^{imp}(\beta) = \text{Tr} G_{mm'}^{0,loc}(\beta), \quad (11)$$

where  $G_{mm'}^{0,loc}$  is local non interacting Green function. Some of LDA+DMFT works treated double counting energy  $E_{dc}$  as a free parameter. The authors of Ref. [25] found that most of described  $\hat{H}^{DC}$  terms proposed in the literature are not completely satisfactory in the case of charge transfer insulator NiO and proposed a *numerical* way to define the necessary double counting correction.

Another possible solution of the double counting problem is to perform Hartree+DMFT or Hartree-Fock+DMFT calculations [26]. While performing Hartree-Fock band structure calculations for real materials we do know exactly what portion of interaction is included. Since diagrammatic expression for Hartree or Hartree-Fock terms are well known, one can calculate them directly and get double counting correction

energy explicitly. However, up to now we are unaware of any Hartree+DMFT or Hartree-Fock+DMFT calculations for real materials.

Completely independent branch of *ab initio* DMFT calculations is GW+DMFT method, which uses instead of density functional theory the so called chain of Hedin equations truncated in a simplest manner by the neglect of vertex corrections (for review see Ref. [22,27]). Because of purely diagrammatic nature of GW there is a natural way to calculate the local part of corresponding Hartree contribution, which can be used as the double counting correction term for GW+DMFT. [27].

### III. CONSISTENT LDA'+DMFT APPROACH

Recently we proposed the LDA'+DMFT approach, which defines consistent parameter free way to avoid the double counting problem [12]. The main idea is to exclude explicitly exchange-correlation energy from self-consistent LDA calculations only for correlated bands. As described above main obstacle to express double counting term exactly is exchange correlation  $E_{xc}^{LDA}(\rho(\mathbf{r}))$  portion of interaction within LDA. So it seems somehow inconsistent to use it to describe correlation effects in narrow (strongly correlated) bands from the very beginning, as these should be treated via more elaborate schemes like DMFT. To overcome this difficulty for these states, we propose to redefine charge density (5) in  $E_{xc}^{LDA}$  as follows:

$$\rho'(\mathbf{r}) = \sum_{i \neq i_d} |\varphi_i(\mathbf{r})|^2 \quad (12)$$

*excluding the contribution of the density of strongly correlated electrons.*

In principle  $E_{xc}^{LDA}$  is not an additive function of charge density. Thus splitting of charge density into two parts may lead to some loss of hybridization between correlated and uncorrelated states. However as we show below this approximation is rather good. Later on we will see that LDA' bands practically do not change their shape with respect to LDA ones for all considered systems. That tells us that "hybridization" is almost not affected by LDA'. The main effect is increase of splitting between oxygen 2p and metal 3d states. It comes from more repulsive potential appearing in the LDA' case since part of exchange correlation energy is excluded there.

Then this redefined  $\rho'(\mathbf{r})$  (12) is used to obtain  $E_{xc}^{LDA}$  and perform the self-consistent LDA' band structure calculations for correlated bands. This procedure leaves out of interaction for correlated states on the LDA' stage just the Hartree contribution (3). Thus, double counting correction term should be consistently taken in the form of the Hartree like term, given by Eq. (8). This  $H_{FLL}^{DC}$  definition also does not have any free parameters. Actually, our approach is in precise correspondence with the standard definition of correlations, as interaction corrections "above" the Hartree-Fock. At the same time all

other states (not counted as strongly correlated) are to be treated with the full power of DFT/LDA and *full*  $\rho$  in  $E_{xc}^{LDA}$ .

Despite the fact that the LDA'+DMFT method is apparently most consistent with the use of FLL type of double counting, in principle all mentioned above definitions of  $H^{DC}$  can also be exploited within LDA'+DMFT. Also there is another "degree of freedom left" – the occupancy  $n_d$ , used in FLL equation, can be obtained either from LDA or LDA' results, or it can be calculated self consistently during the DMFT loop. We used all these variants in our calculations for different compounds presented below. Corresponding values of  $E_{dc}$  listed in Table I. Notations are: FLL(SC) for self consistently calculated  $n_d$  and for  $n_d$  from LDA or LDA' – FLL(LDA). In general FLL(SC) and FLL(LDA) do not differ very much from each other, except for the case of CoO (see below). However, FLL(SC) gives slightly better agreement with experiments. Most Figures presented below are plotted for the FLL(SC) case. We observed that FLL(SC) calculations require more computational time than FLL(LDA).

Thereby our consistent LDA'+DMFT approach is a kind of compromise between Hartree-Fock and DFT/LDA starting points to be followed by DMFT calculations. It was demonstrated in Ref. [12] that this LDA'+DMFT method works perfectly for insulating NiO system, directly producing charge transfer insulator solution, while conventional LDA+DMFT (with FLL) gives metallic solution (cf. Ref. [25]).

## IV. CHARGE TRANSFER INSULATORS

### A. LDA and LDA' band structures

Typical examples of charge transfer insulator (CTI) materials are transition metal monoxides MnO, CoO and NiO. These oxides have rock salt crystal structure with lattice parameters  $a=4.426\text{\AA}$ ,  $4.2615\text{\AA}$  and  $4.1768\text{\AA}$  correspondingly. To obtain LDA and LDA' band structures for MnO, CoO and NiO the linearized muffin-tin orbitals (LMTO) basis set [28] was used. In the corresponding program package TB-LMTO v.47 the  $E_{xc}^{LDA}$  was taken in von Barth-Hedin form [9]. Total and partial densities of states (DOS) together with band dispersions can be seen in Fig. 1 for LDA (dashed lines) and LDA' (solid lines). From top to bottom on Fig. 1 there are MnO, CoO and NiO systems. As reported earlier for NiO [12] LDA' approach changes charge transfer energy  $|E_d - E_p|$ , where  $E_d$  and  $E_p$  are, roughly speaking, one electron energy positions of transition metal 3d and O-2p bands. In Fig. 1 the same tendency for MnO and CoO oxides is seen. For MnO it increases about 0.5 eV and for CoO about 1 eV, similar to NiO. Almost rigid shift of O-2p bands down in energy is observed here, while transition metal 3d states remain almost the same near the Fermi level.

One should mention that (to our knowledge) transi-



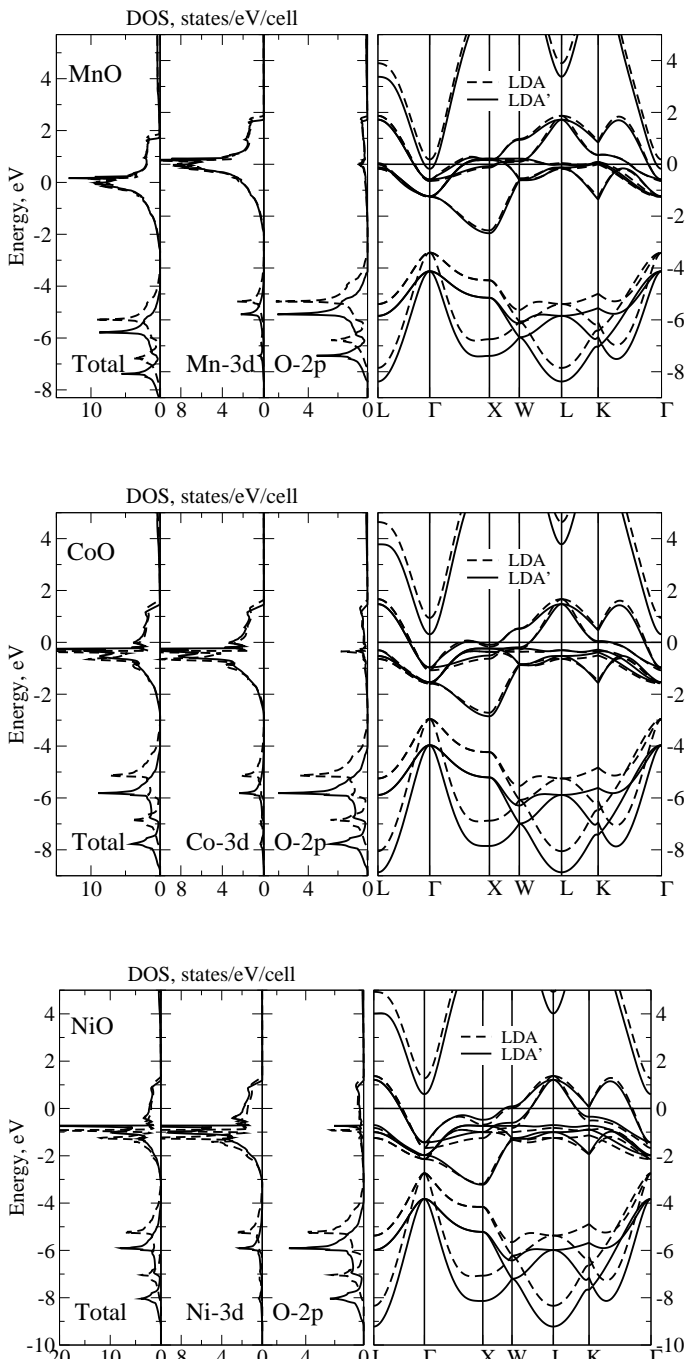


FIG. 1: LDA (dashed lines) and LDA' (solid lines) densities of states (DOS) and band dispersions for MnO (upper row), CoO (middle row) and NiO (lower row). Fermi level is zero.

tion metal 4s states were never included previously into LDA+DMFT calculations for these transition metal oxides. Apparently, this happened because they were reasonably assumed to be weakly correlated and thus projected out from corresponding LDA Hamiltonian. However, transition metal 4s states are rather close to the Fermi level for LDA bands and getting even closer for LDA' ones. They can be seen on Fig. 1 as lowest unoc-

cupied states which are touching the Fermi level for MnO near  $\Gamma$ -point and less than 1eV above the Fermi level for CoO and NiO.

### B. LDA+DMFT and LDA'+DMFT spectral functions

Everywhere in this paper we employ Hirsh-Fye quantum Monte-Carlo algorithm [29] as impurity solver for DMFT equations. To set up DMFT lattice problem we use corresponding LDA and LDA' Hamiltonians, which include all states (without any projecting, as was done e.g. Ref. [24]). Inverse temperature was taken  $\beta = 5\text{eV}^{-1}$ , with 80 time slices for NiO, while for MnO and CoO we used  $\beta = 10\text{eV}^{-1}$  with 120 and 160 time slices respectively. Monte Carlo sampling was done with  $10^6$  sweeps. The use of rather high temperatures does not lead to any qualitative effects in the results, allowing us to avoid unnecessary computational efforts. Parameters of Coulomb interaction were chosen as typical for MnO, CoO and NiO [16,25]:  $U=8$  eV and  $J=1$  eV. Both FLL(SC) and FLL(LDA) double counting definitions were applied for all materials. Respective  $E_{dc}$  values are given in Table I.

To obtain DMFT(QMC) densities of states (DOS) at real energies, we employed the maximum entropy method (MEM) [30]. Then one can get DMFT self-energy on the real frequency axis by using Pade approximants for analytical continuation. Further on it was checked that "Pade" DOS'es are identical to "MEM" DOS'es. Once  $\Sigma(\omega)$  is obtained, one can input it into Eq. (2) and obtain the spectral density function  $A(\mathbf{k}, \omega) = -\frac{1}{\pi} \text{Im}G(\mathbf{k}, \omega)$ . Corresponding maps of spectral density functions, representing effective band structure of these compounds, are given in Fig. 2. Left column of Fig. 2 presents LDA+DMFT results and the right one – LDA'+DMFT for MnO (upper panels), CoO (middle panels) and NiO (lower panels).

### C. LDA+DMFT and LDA'+DMFT DOS

In Fig. 3 we present densities of states obtained by LDA+DMFT (dashed lines) and LDA'+DMFT (solid lines). The left panel corresponds to MnO, middle one to CoO and the left one to NiO. Upper row shows total densities of states, while in other rows we show the contributions of the most important electron states –  $t_{2g}$  and  $e_g$  subshells for 3d transition metal, oxygen 2p states and also transition metal 4s states.

First we focus on MnO case which is perhaps the simplest one among these three. The O-2p states are located between -9 and -4 eV (see Figs. 2 and 3). Then comes lower Hubbard band, which consists of Mn-3d  $t_{2g}$  and  $e_g$  contributions at -4eV and -2.3 eV correspondingly. On spectral function maps LHB is rather wide non dispersive band at these energies. Then we see the so called

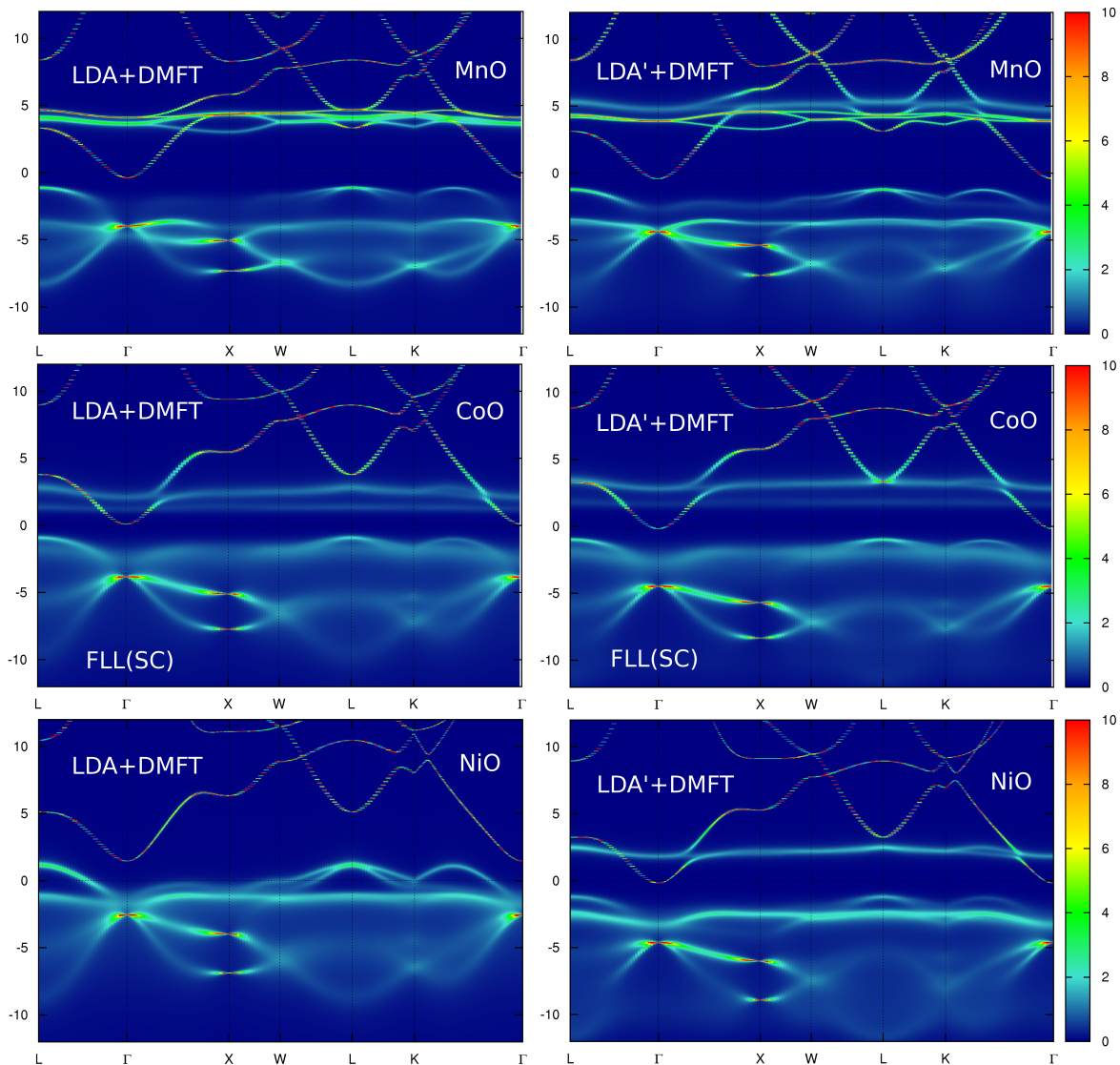


FIG. 2: (Colour online) Comparison of LDA+DMFT (left column) and LDA'+DMFT (right column) calculated spectral density functions for MnO (upper row), CoO (middle row) and NiO (lower row), with FLL(SC) double counting correction. Fermi level is zero.

Zhang-Rice band – the bound state which appears when strongly interacting band is hybridized with charge reservoir. This band can be seen as a peak at  $-1.5$  eV in O-2p states together with Mn-3d  $e_g$  states. Then, between the Zhang-Rice band and the upper Hubbard band there is a gap for Mn-3d states about 3.5 eV for both LDA+DMFT and LDA'+DMFT, which agrees pretty well with experimental spectra (see below). UHB is located above 4 eV and, where  $t_{2g}$  and  $e_g$  contributions can not be separated in energy.

Spectral density map of Fig. 2 (upper row) show some rather well defined band of MnO, which touches the Fermi level in the  $\Gamma$ -point. This band is nothing else but Mn-4s. It is seen from Fig. 3, that most of the Mn-4s spectral weight is actually well above 5 eV. Below there is some rather low intensity tail, which goes through the

gap between the upper Hubbard band and the Zhang-Rice band. Its intensity is at least one order of magnitude lower, than intensities of other contributions to DOS.

Consider next CoO (middle row of Fig. 2 and middle panel of Fig. 3). We see that both LDA+DMFT and LDA'+DMFT results are quite similar. There is some difference in the UHB, where Co-3d  $t_{2g}$  and  $e_g$  contributions can now be separated and in Fig. 3 two almost nondispersive bands around 2 and 3 eV above the Fermi level are clearly seen. The gap between Zhang-Rice band and UHB is about 0.5 eV larger (about 4 eV) for LDA'+DMFT results.

One should note, that LDA+DMFT calculation with FLL(LDA) double counting produces the metallic solution for CoO, as seen from Fig. 4, which qualitatively contradicts the experiments. On the contrary,

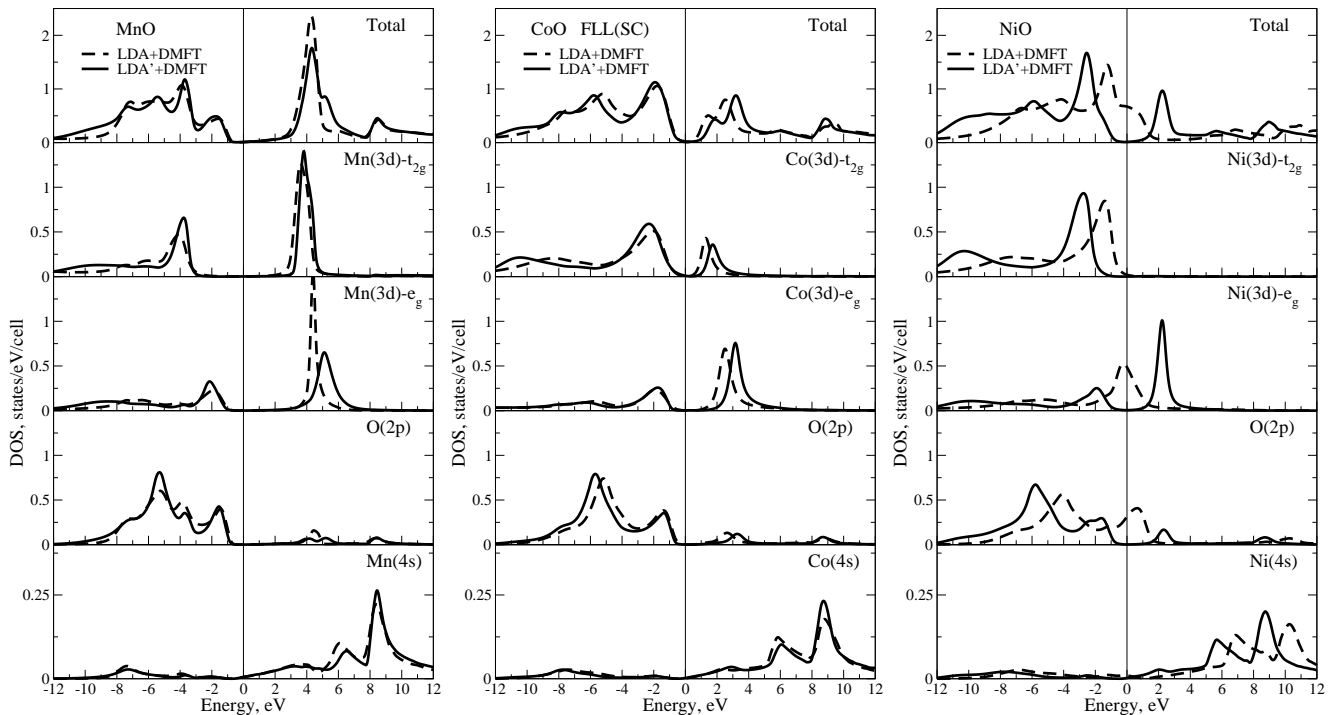


FIG. 3: Comparison of LDA+DMFT (dashed lines) and LDA'+DMFT (solid lines) densities of states for MnO (left panel), CoO (middle panel) and NiO (right panel), with FLL(SC) double counting correction. Fermi level is zero.

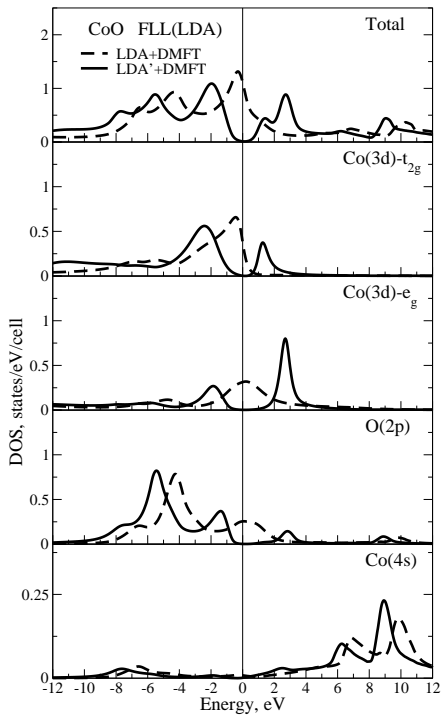


FIG. 4: Comparison of LDA+DMFT (dashed lines) and LDA'+DMFT (solid lines) calculated densities of states for CoO with FLL(LDA) double counting correction. Fermi level is zero.

LDA'+DMFT gives the correct insulating state.

Note, that both in CoO and NiO the behavior of 4s bands is similar to that discussed above for the case of MnO. Spectral density maps of Fig. 2 show the presence of these bands within the charge transfer gap, though the partial density of states due to these bands within the gap is almost negligible (cf. Fig. 3).

To sum up, we stress that both MnO and CoO within LDA'+DMFT are consistently demonstrated to be charge transfer insulators (in contrast to the conventional LDA+DMFT in the case of CoO). The similar behavior was obtained earlier for NiO in Ref. [12]. Here we presented more complete LDA'+DMFT results for NiO, with both FLL(LDA) and FLL(SC) double counting corrections. Conventional LDA+DMFT calculations predict NiO to be metallic in contrast to experiment, while LDA'+DMFT gives charge transfer insulating solution for NiO for both FLL(LDA) and FLL(SC) double counting correction. All other features of NiO LDA'+DMFT band structure are quite similar to MnO and CoO compounds described above.

#### D. LDA+DMFT and LDA'+DMFT optical conductivity

Metallic or insulating behavior can be explicitly demonstrated by calculations of optical conductivity. Below we present our results for optical conductivity behavior of MnO, CoO and NiO within LDA+DMFT and

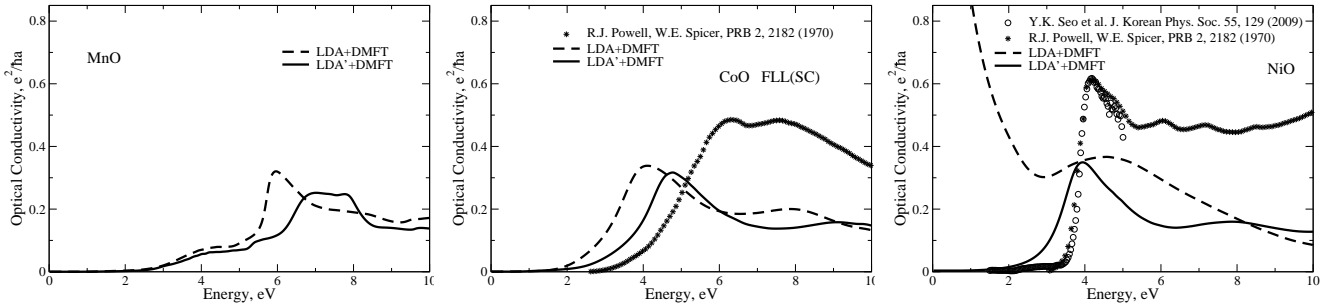


FIG. 5: Comparison of experimental (circles, stars) and calculated LDA+DMFT (dashed lines) and LDA'+DMFT (solid lines) optical conductivities for MnO (left panel), CoO (middle panel) and NiO (right panel).

LDA'+DMFT, allowing us also to analyze the influence of transition metal 4s states on dielectric properties of these oxides. In our calculations we used the following expression for optical conductivity, valid in DMFT [31]:

$$\sigma_{xx}(\omega) = \frac{\pi e^2}{2\hbar a} \int_{-\infty}^{\infty} d\varepsilon \frac{f(\varepsilon) - f(\varepsilon - \omega)}{\omega} \times \frac{1}{N} \sum_{ij\vec{k}\sigma} \left( \frac{\partial \varepsilon_{\vec{k}}^i}{\partial k_x} \right) \left( \frac{\partial \varepsilon_{\vec{k}}^j}{\partial k_x} \right) A_{\vec{k}}^{ij}(\varepsilon) A_{\vec{k}}^{ji}(\varepsilon - \omega) \quad (13)$$

Here  $e$  is electron charge,  $a$  is the lattice constant of corresponding compound,  $f(\varepsilon)$  - Fermi function,  $\varepsilon_{\vec{k}}$  - band dispersion,  $A_{\vec{k}}^{ij}(\varepsilon)$  corresponding (LDA+DMFT or LDA'+DMFT) spectral density function matrix ( $i, j$  are the band indices). During our calculations we found that main contribution to optical conductivity is due to intra-orbital optical transitions. Inter-orbital optical transitions give less than 5% of optical conductivity intensity in frequency range used in our calculations. Also in the present work we neglect possible effects due to optical matrix elements. Calculated theoretical curves obtained in conventional LDA+DMFT (dashed line) and within LDA'+DMFT (solid line) are presented in Fig. 5 for MnO (left panel), CoO (middle panel) and NiO (right panel).

From Fig. 5 we see, that within LDA'+DMFT (solid line) all materials are insulators. Despite the presence of transition metal 4s states close to the Fermi level, possible Drude peak due to these states is not observed. Conventional LDA+DMFT optical conductivity for NiO shows typical metallic behavior, as discussed earlier in the context of DOS behavior.

Now we compare our theoretical results with available experimental data (with an exception of MnO, where we are not aware of any experimental results) [32,33]. In Ref. [32] only experimental data for optical constants  $n(\omega)$  and  $k(\omega)$  were presented. The optical conductivity in units of  $\frac{e^2}{\hbar a}$  (which is about  $5.8 \times 10^3 \Omega^{-1} cm^{-1}$  for given monooxides) can be recalculated from these data using as  $\sigma(\omega) = \frac{n(\omega)k(\omega)}{2\pi} \omega \alpha^{-1} \frac{a}{c}$ , where  $\alpha$  is fine structure constant,  $a$  - lattice constant and  $c$  - speed of light.

Corresponding curves are shown in Fig. 5 by stars. For NiO there are more recent experimental data of Ref. [33], shown with circles. One observes that below the leading absorption edge for CoO and NiO there exist rather long absorption tails with low intensity. We associate these tails with contribution of Co and Ni 4s states. For NiO the overall agreement of LDA'+DMFT results with experimental data is quite satisfactory. For CoO theoretical absorption edge is about 1 eV lower than experimental one. However, this can probably be corrected introducing the larger value of Coulomb interaction  $U$ . Recent constrained RPA study produced it to be 10.8 eV [23], in contrast to 8 eV used in our calculations.

### E. Comparison of LDA+DMFT and LDA'+DMFT results with X-ray experiments

Now we compare our results for DOS with XPS and BIS experiments of Refs. [34–37]. In Fig. 6 LDA+DMFT (dashed lines) and LDA'+DMFT (solid lines) valence and conduction bands spectra are directly compared with spectra for MnO (upper panel), CoO (middle panel) and NiO (lower panel). Theoretical spectra were obtained by multiplication of DOS by Fermi distribution and Gaussian broadening with experimental temperature and resolution.

General structure of spectra is similar for all three compounds. From -14 to -4 eV there are O-2p states, then comes lower Hubbard band at about -3 eV. On the high energy slope of the LHB there we can see a shoulder-like structure, which is nothing else but Zhang-Rice band. Around the Fermi level there is insulating gap. The size of the gap is very well reproduced for MnO by both LDA+DMFT and LDA'+DMFT. For CoO it looks like  $U$  value chosen is a bit too small (as discussed earlier), however LDA'+DMFT spectra gives gap size closer to the experiment. For NiO conventional LDA+DMFT gives metallic solution, while LDA'+DMFT produces CTI solution with correct energy gap size. Experimental positions of the upper Hubbard bands are rather well described by LDA'+DMFT. Since experimental data for NiO goes far above the Fermi level one can identify these



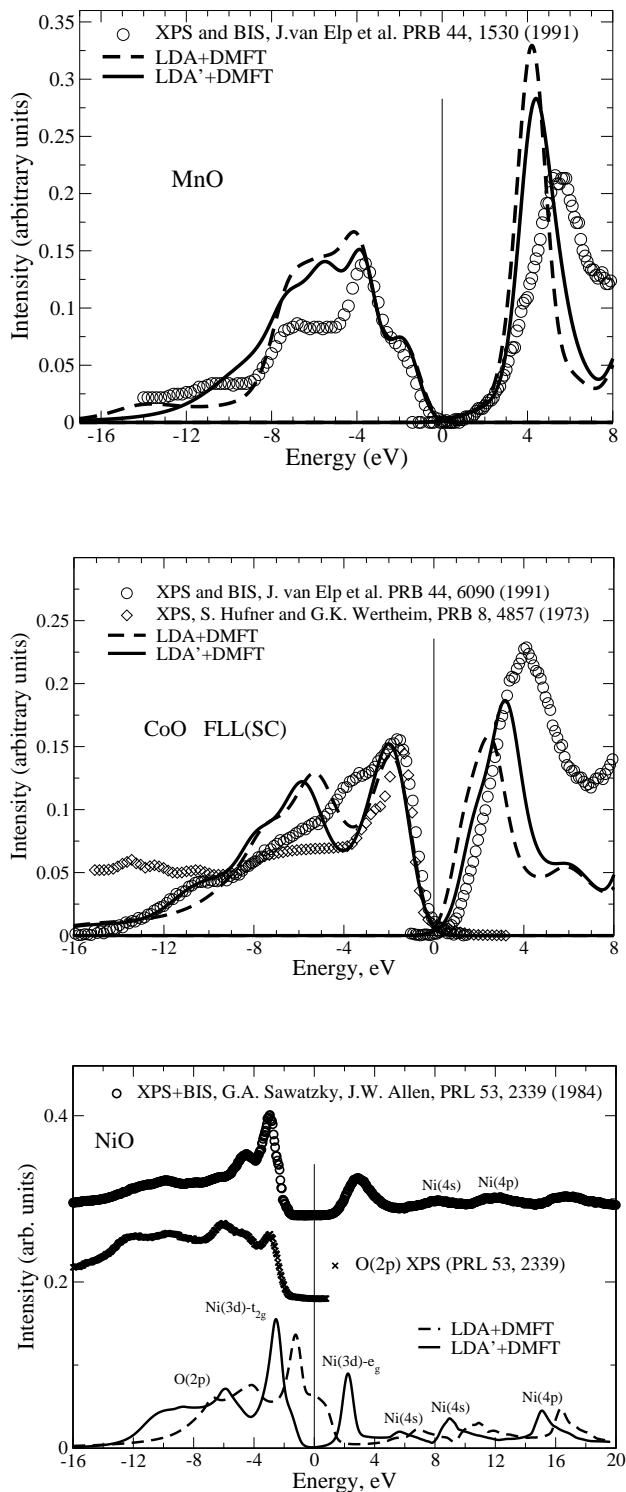


FIG. 6: Comparison of LDA+DMFT (dashed lines) and LDA'+DMFT (solid lines) spectra with XPS and BIS experimental data (circles, diamonds, crosses) for MnO (upper panel), CoO (middle panel) and NiO (lower panel). Fermi level is zero.

high energy structures as Ni-4s and Ni-4p states contributions.

On Fig. 6 one can see that experimental conduction band low energy threshold has a rather long low intensity tail which goes down to the Fermi level. Because of that there is some asymmetry of the gap. We suggest that this asymmetry of the gap originates from transition metal 4s states, which touch the Fermi level from above, as described earlier.

## V. STRONGLY CORRELATED METALS

### A. LDA and LDA' band structure

Strontium vanadate  $\text{SrVO}_3$  is perhaps one of the most simple paramagnetic strongly correlated metallic systems. There is no wonder that it is widely used as a test system for various LDA+DMFT based numerical techniques [38–41].  $\text{SrVO}_3$  has ideal cubic perovskite structure with one d-electron in V-3d shell within triply degenerated  $t_{2g}$  subshell. LDA and LDA' band structure calculations are performed as described in Refs. [38–41] via LMTO method with von Barth-Hedin exchange correlation energy [9].

The 3d bands of vanadium cross the Fermi level, while oxygen 2p states are at  $-8 - -2$  eV i.e. much lower than the Fermi level (see Fig. 7, left panel, dashed lines). If we exclude  $E_{xc}^{LDA}$  contribution for V-3d states as described in Sec. III, we obtain the LDA' band structure shown in Fig. 7 (left panel, solid lines). Similar to Ref. [12] within LDA' approach energy splitting between V-3d and O-2p bands  $|E_d - E_p|$  becomes larger, than in conventional LDA. Since the total number of electrons is fixed, the increase of  $|E_d - E_p|$  LDA' is related to O-2p bands going down in energy by about 0.5 eV, with V-3d states remaining almost unchanged. One should mention here also, that the overall bandshapes are practically not changed in comparison with the conventional LDA bands. The same is true of course for densities of states presented on the left panel of Fig. 7.

Another example of paramagnetic strongly correlated metallic system widely treated by LDA+DMFT is  $\text{Sr}_2\text{RuO}_4$  with Ru-4d<sup>4</sup>  $t_{2g}$  subshell (see Ref. [42] and references therein).  $\text{Sr}_2\text{RuO}_4$  is a layered perovskite with an ideal body-centered tetragonal crystal structure. For LDA and LDA' calculations we used settings described in Ref. [42]. LDA (dashed lines) and LDA' (solid lines) band dispersions and DOS'es are plotted in Fig. 7 (right panel). The picture here is not that simple as for  $\text{SrVO}_3$ . The Ru-4d states, crossing the Fermi level, almost preserve their energy positions and dispersions within LDA'. However LDA' leads to  $|E_d - E_p|$  splitting, because of non-uniform narrowing of O1-2p and O2-2p states, together with the slight shift of O2-2p states. In total  $|E_d - E_p|$  energy splitting is about 0.5 eV larger for LDA' than in conventional LDA.

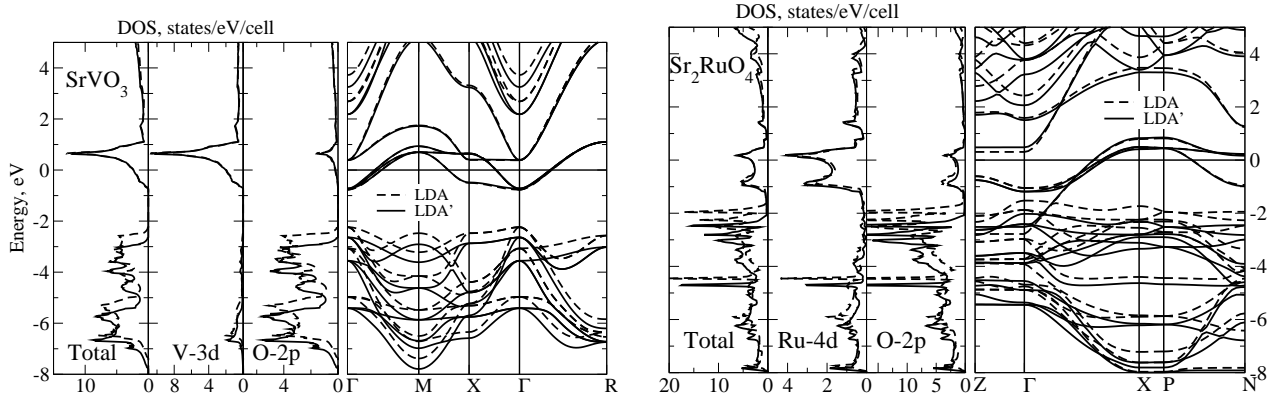


FIG. 7: LDA (dashed lines) and LDA' (solid lines) band dispersions for SrVO<sub>3</sub> (left panel) and Sr<sub>2</sub>RuO<sub>4</sub> (right panel). Fermi level is zero.

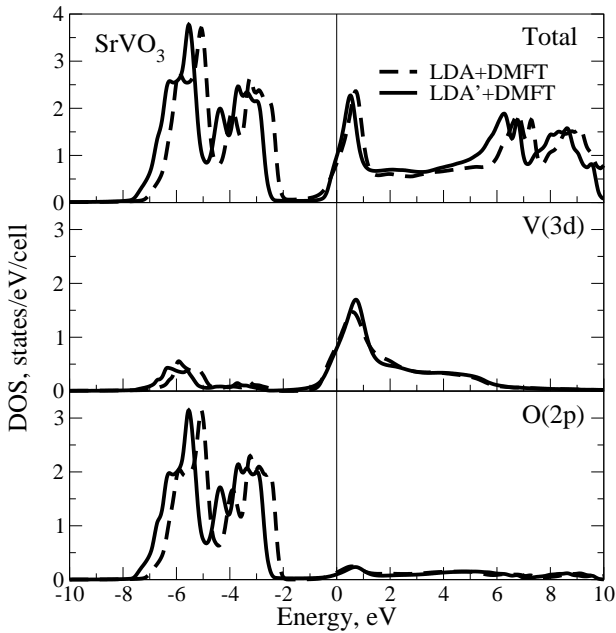


FIG. 8: Densities of states calculated with LDA+DMFT (dashed lines) and LDA'+DMFT (solid lines) for SrVO<sub>3</sub>: V-3d states - upper panel, O-2p states - lower panel. Fermi level is zero.

### B. LDA+DMFT and LDA'+DMFT DOS

In contrast to previous works (Refs. [38–42]) we used here the full TB-LMTO-ASA calculated LDA and LDA' Hamiltonians, employing none of the widely used projection techniques. In QMC calculations inverse temperature was taken to be  $\beta = 10\text{eV}^{-1}$ , with 80 time slices for SrVO<sub>3</sub>, while for Sr<sub>2</sub>RuO<sub>4</sub> we used  $\beta = 15\text{eV}^{-1}$ , with 64 time slices. Coulomb parameters were taken to be  $U=6.0$  eV and  $J=0.7$  eV [24] for SrVO<sub>3</sub> and 3.2 eV and 0.7 eV for Sr<sub>2</sub>RuO<sub>4</sub> respectively [42]. Number of Monte Carlo sweeps was of the order of  $10^6$ . To obtain DMFT(QMC) [29] densities of states at real energies, we again employed

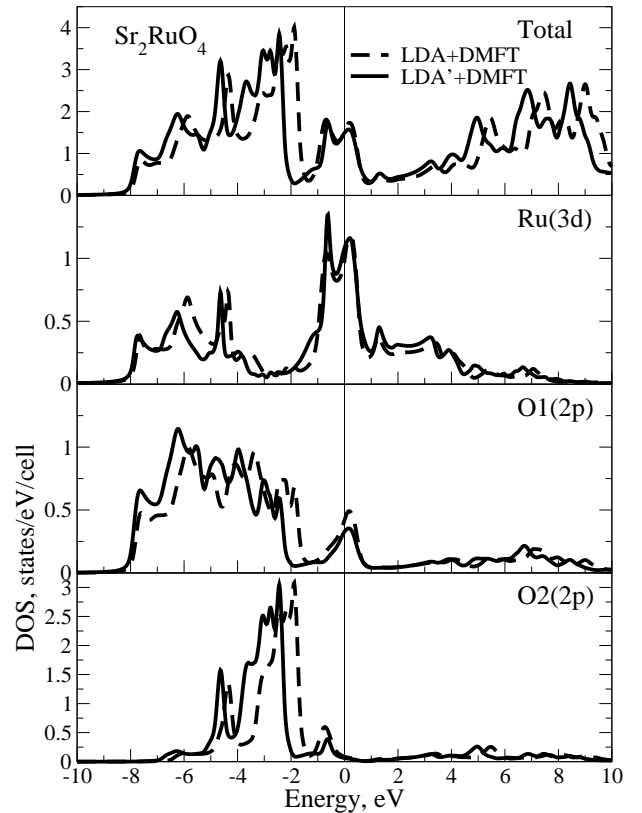


FIG. 9: Densities of states calculated with LDA+DMFT (dashed lines) and LDA'+DMFT (solid lines) for Sr<sub>2</sub>RuO<sub>4</sub>: Ru-4d states - upper panel, O-2p states - middle and lower panels. Fermi level is zero.

the maximum entropy method [30]. To get corresponding DMFT O-2p densities of states the method of Pade approximants was applied to do analytic continuation for DMFT self-energy from Matsubara to real frequencies, with further crosschecking of “MEM” and “Pade” DOS'es to ensure the quality of restored self-energy for real frequencies.

In Figs. 8 and 9 we present the total and par-

tial densities of states for  $\text{SrVO}_3$  and  $\text{Sr}_2\text{RuO}_4$  calculated by the conventional LDA+DMFT (dashed lines) and LDA'+DMFT (solid lines). For both systems LDA'+DMFT results show lower positions of O-2p states in comparison with LDA+DMFT. However, for  $\text{Sr}_2\text{RuO}_4$  it does not reduce just to a rigid shift of oxygen states by about 0.5 eV, as in the case of  $\text{SrVO}_3$ , but is the combination of some small shift with non-uniform narrowing of oxygen bands. Thus, for  $\text{Sr}_2\text{RuO}_4$  only the high energy threshold of O-2p states moves down by 0.5 eV.

As opposed to Refs. [38–41] in both calculations for  $\text{SrVO}_3$  we observe very smooth upper and lower Hubbard bands in V-3d DOS (upper panel of Fig. 8). This agrees well with the full orbital calculations reported in Ref. [24]. Also in Ref. [24] it is shown that smaller value of  $E_{dc}$  (if  $E_{dc}$  is treated as free parameter) moves oxygen states down in energy, which leads to better agreement with experiment (see the next paragraph).

### C. Comparison of LDA+DMFT and LDA'+DMFT results with X-ray experiments

In Figs. 10 and 11 LDA+DMFT (dashed lines) and LDA'+DMFT (solid lines) calculated spectra for  $\text{SrVO}_3$  and  $\text{Sr}_2\text{RuO}_4$  correspondingly are drawn. To get theoretical spectra from total DOS Gaussian broadening to simulate experimental resolution and Lorentzian broadening to simulate lifetime effects together with multiplication with Fermi distribution function were performed as described elsewhere [38–42]. On the figures emission (left side) and absorption (right side) spectra are plotted.

For both systems we have reasonable agreement with experimental data (circles) for valence and conduction bands [39,43–45] (see Figs. 10, 11). However strength of quasiparticle peak is a bit overestimated for valence band and underestimated for conduction band in both LDA+DMFT and LDA'+DMFT methods. The LDA'+DMFT results give slightly better energy position of O-2p states in comparison to LDA+DMFT. In general obtained by LDA'+DMFT results are in agreement with previous LDA+DMFT works (see Refs. [38–42]).

To demonstrate presence of well known lower Hubbard band at -1.5 eV for  $\text{SrVO}_3$  [38–41] on left panel of Fig. 10 V-3d  $t_{2g}$  contribution is shown by cyan line. In Fig. 10 (right panel) for  $\text{SrVO}_3$  instead of upper Hubbard band around 2.5 eV LDA'+DMFT shows rather broad shoulder. This shoulder is formed by  $t_{2g}$  (solid cyan line) and  $e_g$  (dot-dash cyan line) V-3d contributions which corresponds to previous works [38–41]. However the  $e_g$  subband in our case is also modified by correlations. It is shifted up on about 1 eV (as should be for completely empty states) and it has smaller width compared to the LDA one. For  $\text{Sr}_2\text{RuO}_4$  it is known that correlations lead to formation of lower Hubbard band satellite near -3 eV [42]. This satellite is also seen in the LDA'+DMFT results on the right panel of Fig. 11 and is formed essentially by Ru-4d  $t_{2g}$  states (cyan line).

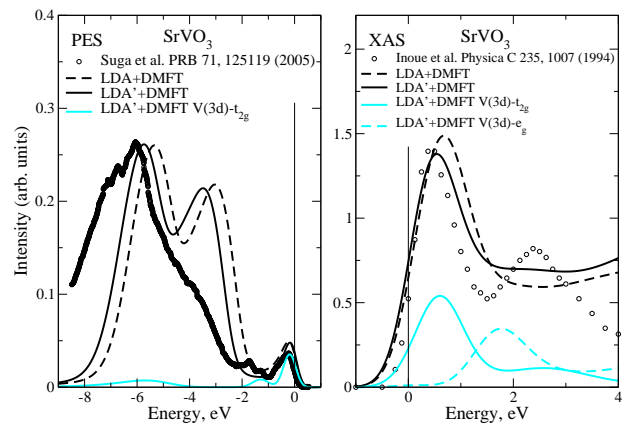


FIG. 10: (Colour online) Comparison of LDA+DMFT (dashed lines) and LDA'+DMFT (solid lines) calculated spectra for  $\text{SrVO}_3$  with experimental data. With cyan colour LDA'+DMFT  $t_{2g}$  (solid line) and  $e_g$  (dot-dash line) V-3d contributions are shown. Fermi level is zero.

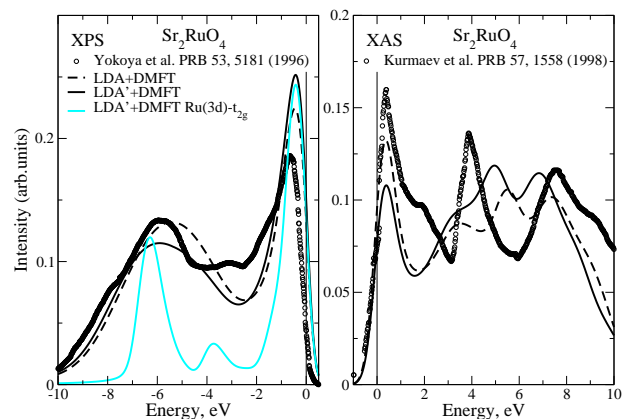


FIG. 11: (Colour online) Comparison of LDA+DMFT (dashed lines) and LDA'+DMFT (solid lines) calculated spectra for  $\text{Sr}_2\text{RuO}_4$  with experimental data. With cyan colour LDA'+DMFT  $t_{2g}$  Ru-4d contribution is shown. Fermi level is zero.

## VI. 5. CONCLUSION

This work continues our research of the double counting problem arising within the LDA+DMFT computational scheme. The problem appears because some portion of local electron-electron interaction is already present in LDA calculations. Since DMFT gives exact local solution of the Hubbard-like model one should avoid double counting between LDA and DMFT local electronic interactions. Despite 15 years of developing of the LDA+DMFT method still there are no unique definition of this double counting term. This happens because LDA contribution to exchange correlation energy has no diagrammatic expression. Several different *ad hoc* definitions which are available now work well only in some particular cases, for some particular compounds. Sometimes one can get even qualitatively wrong LDA+DMFT

solution if double counting term is chosen not careful enough. To overcome this problem we proposed consistent LDA'+DMFT approach [12]. It uses natural assumption of explicit exclusion of LDA exchange correlation potential for correlated electronic shells since anyhow exchange-correlation effects will be accounted later by DMFT. Then local interactions left out for correlated states in the LDA' are only Hartree ones. After that corresponding double counting term of the LDA'+DMFT Hamiltonian consistently must be taken in the local Hartree form (FLL form).

With this paper we present extensive LDA'+DMFT investigation of typical representatives of two wide classes of strongly correlated systems in the paramagnetic phase: strongly correlated metals (SrVO<sub>3</sub> and Sr<sub>2</sub>RuO<sub>4</sub>) and charge transfer insulators (MnO, CoO and NiO). For strongly correlated metals where double counting is not that severe LDA'+DMFT agrees well with traditional LDA+DMFT results with FLL double counting type. LDA'+DMFT gives slightly better position of O-2p states in comparison with experiment. LDA'+DMFT results for charge transfer insulators MnO, CoO and NiO are more interesting. CoO and NiO systems are found to be metals within conventional LDA+DMFT calculations while LDA'+DMFT gives proper insulating solution. Transition metal 4s-states missed in previous

LDA+DMFT works on these monooxides are found to be responsible for charge gap asymmetry around the Fermi level.

Finally one can conclude that proposed by us consistent LDA'+DMFT method works well for both metallic and insulating systems. We believe that our LDA'+DMFT provides reasonable parameter free treatment of the double counting problem.

## VII. ACKNOWLEDGEMENTS

We thank A.I. Poteryaev for providing us QMC code and many helpful discussions. We are grateful to E.Z. Kuchinskii for providing us more insight into calculations of optical conductivity. This work is partly supported by RFBR grant 11-02-00147 and was performed within the framework of programs of fundamental research of the Russian Academy of Sciences (RAS) "Quantum mesoscopic and disordered structures" (12-II-2-1002) and of the Physics Division of RAS "Strongly correlated electrons in solids and structures" (012-T-2-1001). NSP acknowledges the support of the Dynasty Foundation and International Center of Fundamental Physics in Moscow.

- 
- <sup>1</sup> V.I. Anisimov, A.I. Poteryaev, M.A. Korotin, A.O. Anokhin and G. Kotliar, J. Phys. Cond. Matter **9**, 7359 (1997).
- <sup>2</sup> A.I. Lichtenstein, M.I. Katsnelson, Phys. Rev. B **57**, 6884 (1998).
- <sup>3</sup> I.A. Nekrasov, K. Held, N. Blümer, A.I. Poteryaev, V.I. Anisimov and D. Vollhardt, Euro. Phys. J. B **18**, 55 (2000).
- <sup>4</sup> K. Held, I.A. Nekrasov, G. Keller, V. Eyert, N. Blümer, A.K. McMahan, R.T. Scalettar, T. Pruschke, V.I. Anisimov, D. Vollhardt, Psi-k Newsletter **56**, 65 (2003).
- <sup>5</sup> K. Held, I.A. Nekrasov, N. Blümer, V.I. Anisimov and D. Vollhardt, Int. J. Mod. Phys. B **15**, 2611 (2001); K. Held, I.A. Nekrasov, G. Keller, V. Eyert, N. Blümer, A.K. McMahan, R.T. Scalettar, T. Pruschke, V.I. Anisimov, and D. Vollhardt in *Quantum Simulations of Complex Many-Body Systems: From Theory to Algorithms*, (Eds. J. Grotendorst, D. Marks, A. Muramatsu) NIC Series Volume 10 (2002) p. 175; A.I. Lichtenstein, M.I. Katsnelson, G. Kotliar G, in *Electron Correlations and Materials Properties 2nd ed.* (Eds. A. Gonis, N. Kioussis, M. Ciftan) (Kluwer Academic/Plenum, 2002) p. 428.
- <sup>6</sup> V.I. Anisimov, Yu.A. Izyumov, *Electronic Structure of Strongly Correlated Materials* (Berlin - Heidelberg: Springer, 2010).
- <sup>7</sup> B. Amadon, J. Phys.: Condens. Matter **24**, 075604 (2012).
- <sup>8</sup> R. O. Jones and O. Gunnarsson, Rev. Mod. Phys. **61**, 689 (1989).
- <sup>9</sup> L. Hedin and B. Lundqvist, J. Phys. C: Solid State Phys. **4**, 2064 (1971); U. von Barth and L. Hedin, J. Phys. C: Solid State Phys. **5**, 1629 (1972).
- <sup>10</sup> D. M. Ceperley and B. J. Alder, Phys. Rev. Lett. **45**, 566 (1980).
- <sup>11</sup> M. B. Zöfl, Th. Pruschke, J. Keller A. I. Poteryaev, I. A. Nekrasov, and V. I. Anisimov, Phys. Rev. B **61**, 12810 (2000).
- <sup>12</sup> I.A. Nekrasov, N.S. Pavlov, M.V. Sadovskii, Pis'ma v ZhETF **95**, 659 (2012); arXiv:1204.2361.
- <sup>13</sup> V.I. Anisimov, J. Zaanen and O.K. Andersen, Phys. Rev. B **44**, 943 (1991); V. I. Anisimov, F. Aryasetiawan, and A. I. Lichtenstein, J. Phys. Cond. Matter **9**, 767 (1997).
- <sup>14</sup> M.T. Czyżyk and G.A. Sawatzky, Phys. Rev. B, **49**, 14211 (1994).
- <sup>15</sup> O. Gunnarsson, O. K. Andersen, O. Jepsen, and J. Zaanen, Phys. Rev. B **39**, 1708 (1989).
- <sup>16</sup> J. Kunes, V. I. Anisimov, S. L. Skornyakov, A. V. Lukoyanov, and D. Vollhardt, Phys. Rev. Lett. **99**, 156404 (2007); J. Kunes, V. I. Anisimov, A. V. Lukoyanov, and D. Vollhardt, Phys. Rev. B, **75**, 165115 (2007).
- <sup>17</sup> V.I. Anisimov, I.V. Solovyev, M.A. Korotin, M.T. Czyżyk, and G.A. Sawatzky, Phys. Rev. B **48**, 16929 (1993).
- <sup>18</sup> J.-X. Zhu, P. H. Tobash, E. D. Bauer, F. Ronning, B. L. Scott, K. Haule, G. Kotliar, R. C. Albers and J. M. Wills, Europhys. Lett. **97**, 57001 (2012).
- <sup>19</sup> I. Leonov, A. Poteryaev, V. Anisimov, D. Vollhardt, Phys. Rev. Lett. **106**, 106405 (2011).
- <sup>20</sup> V. Anisimov, A. Belozеров, A. Poteryaev, I. Leonov, arXiv:1204.1636.
- <sup>21</sup> A.I. Lichtenstein, M.I. Katsnelson, G. Kotliar, Phys. Rev. Lett. **87**, 067205 (2001); M.I. Katsnelson, A.I. Lichtenstein, Eur. Phys. J. B **30**, 9 (2002).
- <sup>22</sup> F. Aryasetiawan, S. Biermann, and A. Georges, in *Correlation Spectroscopy of Surfaces, Thin Films, and Nanostructures*



- tures, Wiley-VCH Verlag GmbH & Co. KGaA, edited by J. Berakdar, J. Kirschner, p. 1 (2004), ISBN: 3-527-40477-5, arXiv:0401626.
- <sup>23</sup> J. Kunes, V. Krapek, A.V. Kozhevnikov, arXiv:1202.0110.
- <sup>24</sup> B. Amadon, F. Lechermann, A. Georges, F. Jollet, T. O. Wehling, and A. I. Lichtenstein, Phys. Rev. B **77**, 205112 (2008).
- <sup>25</sup> M. Karolak, G. Ulm, T. Wehling, V. Mazurenko, A. Poteryaev, A. Lichtenstein, Journal of Electron Spectroscopy and Related Phenomena, Volume **181**, 11 (2010).
- <sup>26</sup> K. Held, Adv. Phys. **56**, 829 (2007). (see page 862)
- <sup>27</sup> K. Held, C. Taranto, G. Rohringer, and A. Toschi, Hedin Equations, GW, GW+DMFT, and All That in The LDA+DMFT approach to strongly correlated materials - Lecture Notes of the Autumn School 2011 Hands-on LDA+DMFT; eds: E. Pavarini, E. Koch, D. Vollhardt, A. Lichtenstein; publisher: FZ Julich GmbH [arxiv.org/abs/1109.3972].
- <sup>28</sup> O.K. Andersen, Phys. Rev. B **12**, 3060 (1975); O. K. Andersen and O. Jepsen, Phys. Rev. Lett. **53**, 2571 (1984).
- <sup>29</sup> J. E. Hirsch and R. M. Fye, Phys. Rev. Lett. **56**, 2521 (1986); M. Jarrell, Phys. Rev. Lett. **69**, 168 (1992); M. Rozenberg, X. Y. Zhang, and G. Kotliar, Phys. Rev. Lett. **69**, 1236 (1992); A. Georges and W. Krauth, Phys. Rev. Lett. **69**, 1240 (1992); M. Jarrell, in *Numerical Methods for Lattice Quantum Many-Body Problems*, edited by D. Scalapino, Addison Wesley, 1997.
- <sup>30</sup> M. Jarrell and J. E. Gubernatis, Physics Reports **269**, 133 (1996).
- <sup>31</sup> Th. Pruschke, M. Jarrel, and J.K. Freericks. Adv. Phys. **44**, 187 (1995).
- <sup>32</sup> R.J. Powell, W.E. Spicer, Phys. Rev. B **2**, 2182 (1970).
- <sup>33</sup> Y.K. Seo, D.J. Lee, Y. S. Lee, J. Korean Phys. Soc. **55**, 129 (2009).
- <sup>34</sup> J. van Elp, R.H. Potze, H. Eskes, R. Berger, G.A. Sawatzky, Phys. Rev. B **44**, 1530 (1991).
- <sup>35</sup> S. Hufner and G.K. Wertheim, Phys. Rev. B **8**, 4857 (1973).
- <sup>36</sup> J. van Elp, J.L. Wieland, H. Eskes, P. Kuiper, G.A. Sawatzky, F.M.F. de Groot, T.S. Turner, Phys. Rev. B **44**, 6090 (1991).
- <sup>37</sup> G.A. Sawatzky, J.W. Allen, Phys. Rev. Lett. **53**, 2339 (1984).
- <sup>38</sup> A. Sekiyama, H. Fujiwara, S. Imada, S. Suga, H. Eisaki, S.I. Uchida, K. Takegahara, H. Harima, Y. Saitoh, I.A. Nekrasov, G. Keller, D.E. Kondakov, A.V. Kozhevnikov, Th. Pruschke, K. Held, D. Vollhardt, and V.I. Anisimov, Phys. Rev. Lett. **93**, 156402 (2004).
- <sup>39</sup> V.I. Anisimov, D.E. Kondakov, A.V. Kozhevnikov, I.A. Nekrasov, Z.V. Pchelkina, J.W. Allen, S.-K. Mo, H.-D. Kim, P. Metcalf, S. Suga, A. Sekiyama, G. Keller, I. Leonov, X. Ren, and D. Vollhardt, Phys. Rev. B **71**, 125119 (2005).
- <sup>40</sup> I.A. Nekrasov, G. Keller, D.E. Kondakov, A.V. Kozhevnikov, Th. Pruschke, K. Held, D. Vollhardt, and V.I. Anisimov, Phys. Rev. B **72**, 155106 (2005).
- <sup>41</sup> I.A. Nekrasov, K. Held, G. Keller, D.E. Kondakov, Th. Pruschke, M. Kollar, O.K. Andersen, V.I. Anisimov, and D. Vollhardt, Phys. Rev. B **73**, 155112 (2006).
- <sup>42</sup> Z.V. Pchelkina, I.A. Nekrasov, Th. Pruschke, A. Sekiyama, S. Suga, V.I. Anisimov, and D. Vollhardt, Phys. Rev. B **75**, 035122 (2007).
- <sup>43</sup> I.H. Inoue, I. Hase, Y. Aiura, A. Fujimori, K. Morikawa, T. Mizokawa, Y. Haruyama, T. Maruyama, Y. Nishihara, Physica C **235**, 1007 (1994)
- <sup>44</sup> T. Yokoya, A. Chainani, T. Takahashi, H. Katayama-Yoshida, M. Kasai, Y. Tokura, N. Shanthi, D.D. Sarma, Phys. Rev. B **53**, 8151 (1996).
- <sup>45</sup> E.Z. Kurmaev, S. Stadler, D.L. Ederer, Y. Harada, S. Shin, M.M. Grush, T. A. Callcott, R.C.C. Perera, D.A. Zatssepin, N. Ovechkina, M. Kasai, Y. Tokura, T. Takahashi, K. Chandrasekaran, R. Vijayaraghavan, U.V. Varadaraju, Phys. Rev. B **57**, 1558 (1998).

TABLE I: LDA and LDA' occupancies and corresponding values of LDA+DMFT and LDA'+DMFT double counting terms (eV) for systems under consideration.

| Compound                         | $n_{LDA}$ | $n_{LDA'}$ | LDA+DMFT<br>FLL(LDA) | LDA+DMFT<br>FLL(SC) | LDA'+DMFT<br>FLL(LDA) | LDA'+DMFT<br>FLL(SC) |
|----------------------------------|-----------|------------|----------------------|---------------------|-----------------------|----------------------|
| SrVO <sub>3</sub>                | 2.61      | 2.44       | 12.33                | 11.99               | 10.35                 | 10.92                |
| Sr <sub>2</sub> RuO <sub>4</sub> | 5.65      | 5.39       | 14.32                | 14.60               | 12.92                 | 13.73                |
| MnO                              | 5.59      | 5.43       | 39.05                | 35.49               | 36.62                 | 35.30                |
| CoO                              | 7.60      | 7.41       | 54.28                | 50.90               | 51.42                 | 50.49                |
| NiO                              | 8.54      | 8.34       | 60.90                | 62.01               | 57.91                 | 58.13                |